RSC Advances

ROYAL SOCIETY OF CHEMISTRY

www.rsc.org/advances

Graphical Abstract

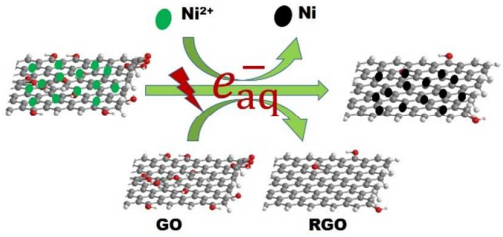

We here demonstrate a facile one-step synthesis of RGO-Ni hybrid materials, where Ni^{2+} ions and GO are simultaneously reduced by γ-irradiation. RGO-Ni, with Ni nanoparticles well dispersed on the RGO surface, shows much enhanced EM absorption ability than the individuals.

RSCPublishing

COMMUNICATION

γ-irradiation induced one-step synthesis of electromagnetic functionalized reduced graphene oxide-Ni nanocomposites

Cite this: DOI: 10.1039/x0xx00000x

Received ooth January 2012,
Accepted ooth January 2012

DOI: 10.1039/x0xx00000x

www.rsc.org/

Hongtao Zhao,[abc*] Zhigang Li,[bc*] Nan Zhang,[bc] Yunchen Du,[b] Siwei Li,[b] Lin Shao,[a] Deyu Gao,[b] Xijiang Han[b] and Ping Xu[b*]

We here demonstrate a facile one-step synthesis of RGO-Ni hybrid materials, where Ni^{2+} ions and GO are simultaneously reduced by γ-irradiation. RGO-Ni, with Ni nanoparticles well dispersed on the RGO surface, shows much enhanced EM absorption ability than the individuals.

Electromagnetic (EM) absorption materials have attracted more and more attention owing to their perspective applications in the areas of electronic industry-wireless devices, advanced electronics, electromagnetic interference.[1-3] Ideal EM absorption material should meet the following demands: thin in thickness, light in weight, wide in adsorption band, and strong in adsorption.[4] The significant parameters that influence the absorbing properties are the complex permeability (μ_r) and permittivity (ε_r).[5] Traditionally, ferrites and magnetic metals such as Fe, Co, Ni and their alloys have been widely considered as promising EM absorption materials owing to their strong complex permeability.[6] However, their high density and large required thickness restrict their universal application in EM-related fields. Through a careful control of the reaction condition, the prepared hierarchical Ni nanostructures themselves only showed a maximum refelction loss of about -10 dB.[7] Consequently, design and successful preparation of materials with lightweight and stable electromagnetic absorption characteristics are urgent and necessary.

In previous reports,[8] nanocomposites consisting of carbon nanotubes (CNTs) and magnetic materials have been exploited as efficient EM absorbers, although the absorbing ability of CNTs itself is relatively weak, and complicated fabrication techniques are required. Compared to CNTs, graphene is an ideal matrix for loading magnetic nanoparticles because of its unique properties, which is a two dimensional sheet of carbon atoms that bond together in a hexagonal lattice possessing high mechanical strength, high thermal conductivity, high electron mobility and high specific surface area.[9] Considering its unique electronic properties, efforts have been made to develop graphene-based EM absorption materials. Chen et al fabricated Fe/graphene nanocomposites and the maximum reflection loss to electromagnetic waves was up to -31.5 dB at 14.2 GHz with a thickness of 2.5 mm.[10] Li et al. has reported the Fe_3O_4–graphene hybrids with reflection loss exceeding -10 dB in 7.5–18 GHz with thicknesses of 1.48–3 mm, accompanying a maximum reflection loss value of -30.1 dB at a 1.48 mm matching thickness and 17.2 GHz matching frequency.[11] Our previous study has shown that reduced graphene oxide (RGO), with the presence of defect and oxygen-containing groups, can display better EM absorption performance than graphite, due to the introduction of additional polarization relaxations.[12]

Herein, we report a one-step facile and clean method to synthesize RGO-Ni nanocomposites via a γ-irradiation technique (see Scheme 1). RGO-Ni nanocomposites, with Ni nanoparticles evenly supported on RGO, can be directly obtained from a solution containing GO and Ni^{2+} ions by a γ-irradiation induced reduction process. The as-fabricated RGO-Ni nanocomposites, combining the synergetic EM absorption effect from RGO (dielectric loss) and Ni (magnetic loss), show enhanced EM absorption perofrmances as compared to the individual components.

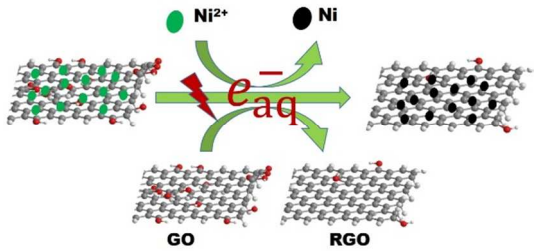

Scheme 1 Schematic illustration of the one-step synthesis of RGO-Ni nanocomposites via a γ-irradiation technique.

Graphite oxide (GO) was prepared using expansible graphite by the pressurized oxidation and multiplex reduction method.[13] In a typical synthesis, a solution of Ni^{2+} ions was added into the GO suspension, and then propanol was added. The solution was bubbled with nitrogen for 30 min to remove dissolved oxygen and then sealed, before it was subjected to γ-irradiation. During the irradiation process, water molecules would be decomposed into both oxidative (hydroxyl radical, ·OH) and reductive (hydrogen and hydrated electrons, H and e_{aq}^-) species.[14, 15] Alcohols introduced into the systemcan eliminate the oxidative species as radical scavengers while keep the useful reductive species,[16] which enable the reduction of GO and Ni^{2+} ions simultaneously to produce RGO-Ni nanocomposites. From Fig. 1a, the RGO nanosheets reduced from GO by γ-irradiation are ultrathin and transparent. The wrinkled and rippled structure has also been observed on highly exfoliated RGO

samples as reported in the literature,[17] which is due to deformation upon the exfoliation and restacking process. Fig. 1b shows the TEM image of the as-prepared RGO-Ni nanocomposites, where the Ni nanoparticles are well dispersed on RGO surface, preferentially populated at the wrinkled and rippled sites. HR-TEM image in Fig. 1c shows that these Ni nanoparticles are highly crystallized. Size histogram in Fig. 1d reveals that these Ni nanoparticles are mostly 8-12 nm in size. Morphology and size features from SEM images agree well with the TEM images (See Fig. S1 in ESI†).

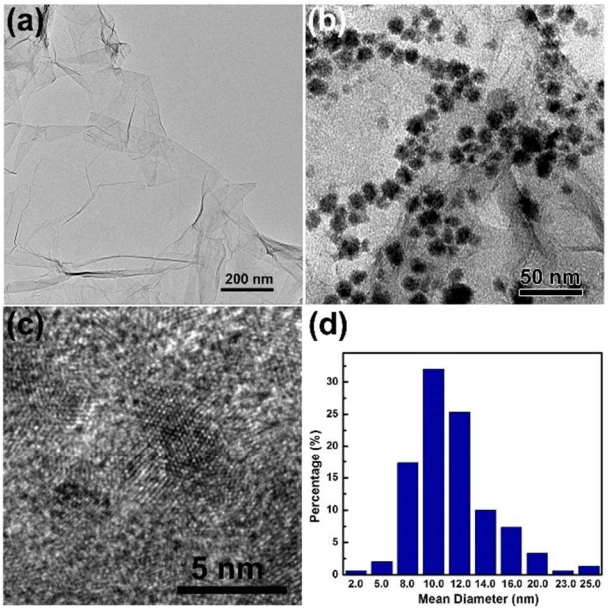

Fig. 1 TEM images of the as-prepared RGO (a) and RGO-Ni nanocomposites (b), HR-TEM images of the RGO-Ni nanocomposites (c), and size distribution of the Ni nanoparticles supported on RGO (d).

Fig. 2a shows the X-ray diffraction (XRD) patterns of the as-prepared samples. A feature diffraction peak of GO at 2θ=10.6° corresponding to the (001) plane appears as the stacking order is observed and the *d*-spacing expanded to 0.85 nm.[18] The reduction of GO into RGO after γ-irradiation can be verified from the disappearance of (001) peak, and the peak at 2θ=23.5°is ascribed to the (002) plane of RGO. For RGO-Ni nanocomposite, the peaks at 2θ=44.42°, 51.82°, and 76.26° can be well indexed to the (111), (200), and (220) (JCPDS 04-0850) planes of face-centered cubic (fcc) Ni crystals. The highly crystallized Ni nanoparticles prevents us from seeing the (002) peak of RGO. The average size of Ni nanoparticles estimated from XRD by Scherrer's equation agrees well with the that found from the TEM images.[19] XRD results have confirmed the simultaneous reduction of Ni^{2+} ions and GO during the γ-irradiation process to produce RGO-Ni nanocomposites.

Raman spectra of the as-prepared samples are shown in Fig. 2b, where G band is mainly assigned to the in-plane displacement of carbon atoms in hexagonal carbon sheets and D band is caused by the disorder in the graphitic structure due to the extensive oxidation and exfoliation.[20] The intensity ratio of D band and G band, I_D/I_G, of RGO (1.72) is higher than that of GO(1.12), which confirms successful reduction of GO as γ-irradiation may introduce more defects.[21, 22] The reduction of GO to RGO can also be manifested by the FT-IR results (see Fig. S2 in ESI†).[23] In the RGO-Ni nanocomposite, a slightly higher I_D/I_G value (1.80) than RGO was found, which might be caused by the interaction of Ni nanoparticles with residual oxygen-containing groups on RGO surface.[24] The as-prepared RGO-Ni sample shows a saturation magnetization of ~ 58 emu/g, which renders an easy collection and separation of the sample from the aqueous phase (Fig. 2c).

The reflection loss (RL) properties of the prepared samples are evaluated by the transmission line theory.[25]

$$RL=20\log\left|\frac{Z_{in}-1}{Z_{in}+1}\right| \quad (1)$$

$$Z_{in}=\sqrt{\mu_r/\varepsilon_r}\tanh[j(2\pi fd/c)\sqrt{\mu_r\varepsilon_r}] \quad (2)$$

where Z_{in} is the normalized input impedance when the electromagnetic wave incidence is normal to the absorber, f is the frequency of the EM wave, d is the thickness of the absorber, and c is the velocity of EM wave in free space. A comparison of the EM absorption properties of GO, RGO, and RGO-Ni samples is displayed in Fig. 2d. As can be seen, GO has very limited EM absorption ability, less than -5 dB across the entire frequency range. RGO, with better EM absorption than GO at lower frequencies (2-11 GHz), shows a maximum RL value of -6.9 dB at 7 GHz. Above results demonstrate that no RL higher than -10 dB can be obtained from the as-prepared GO and RGO materials. However, when RGO surface is decorated with Ni nanoparticles, the EM absorption behaviors at higher frequency ranges (10-18 GHz) can be greatly enhanced. A maximum RL value of -40 dB can be found at 16.6 GHz for RGO-Ni nanocomposites, and in the frequency range of 14.2-18 GHz, all RL values are higher than -10 dB. This EM absorption behavior is comparable to the reported best EM absorption on similar nanocomposite materials.[26, 27]

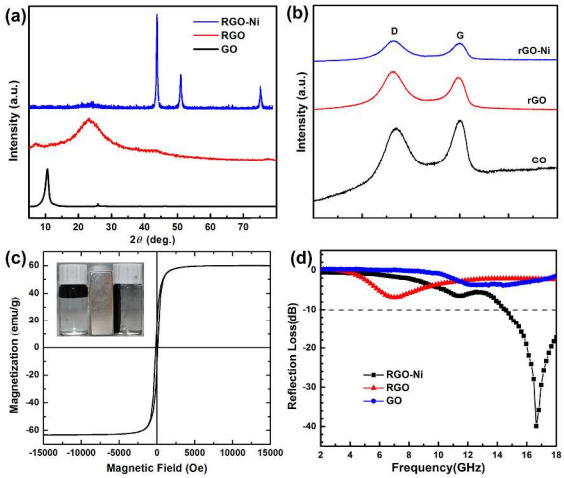

Fig.2 Raman spectra (a), X-ray diffraction (XRD) patterns (b), and EM absorption properties (d) of the prepared GO, RGO, and RGO-Ni nanocomposites. (c) magnetic property of the RGO-Ni nanocomposites.

In order to better understand the EM absorption performances of the as-prepared materials, the EM parameters (μ_r and ε_r) have been outlined in Fig. 3. The real part (ε') and imaginary part (ε'')of permittivity represent the energy storage ability and loss ability, respectively. ε' values of all the samples decrease with the increase in the frequency, and RGO has the highest ε' due to improved conductivity (Fig. 3a). With the decoration of Ni nanoparticles, RGO-Ni has medium ε' values. GO has lowest ε', mainly due to its deteriorated conductivity after a damage of the carbon structures of defect-free graphene. Fig. 3b shows the ε'' values of the prepared samples, which are almost constantly zero in the whole frequency range for GO. After reduction, RGO has tremendously larger ε'' values, which decrease from 33.6 at 2 GHz to 16 at 18 GHz. RGO-Ni shows decreased and steady ε'' values at about 3 in the range of 2-18 GHz. As shown in Fig. 3c, μ' values display no regular rules for the three samples, where GO has the highest values in the whole

frequency range. μ' for RGO-Ni increases from 0.78 at 2 GHz to 1.00 at 10.6 GHz, then decreases sharply to 0.75 at 12.4 GHz, and then increases to 0.87 at 18 GHz. However, from μ'' values in Fig. 3d, one can see that RGO-Ni sample shows enhanced magnetic loss property. RGO and GO mostly are negative in μ'', an indication of no magnetic loss due to the absence of magnetic component in the materials. While, μ'' of RGO-Ni decreases from 0.36 at 2 GHz to 0.05 at 18 GHz, with a peak of 0.15 at 11.6 GHz. A comparison of the dielectric loss ($\varepsilon''/\varepsilon'$) and magnetic loss ($\mu''/\mu'$) demonstrates that besides maintained dielectric loss from RGO, RGO-Ni has much improved magnetic loss from the introduction of Ni nanoparticles (see Fig. S3 and S4 in ESI†).

In a previous work, we have investigated the EM absorption mechanism of RGO materials, where defect polarization relaxation and electronic dipole relaxation due to the presence of defect and oxygen-containing functional groups mainly contribute to the enhanced EM absorption (dielectric loss) behaviors of RGO.[12] Here, for the RGO-Ni hybrid material, dielectric loss is still maintained, and introduction of Ni nanoparticles brings another loss factor, magnetic loss. Moreover, from the ε' values, one can see that the electric conductivity of RGO-Ni should be considerably smaller than that of RGO according to the free electron theory, and thus an improved impedance matching can be expected for the hybrid material, as too high permittivity of absorber is harmful to the impedance matching and results in strong reflection and weak absorption.[28] Therefore, EM absorption of RGO-Ni originates from a synergetic consequence of dielectric loss, magnetic loss and improved impedance matching.

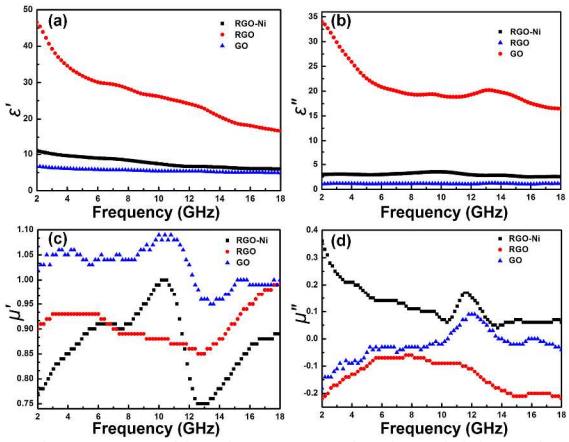

Fig.3 Real part (ε', a) and imaginary part (ε'', b) of permittivity, and real part (μ', c) and imaginary part (μ'', d) of permeability of the prepared GO, RGO, and RGO-Ni nanocomposites.

In summary, we have demonstrated a facile one-step synthesis of electromagnetic functionalized RGO-Ni nanocomposites, where Ni^{2+} ions and GO are simultaneously reduced by the γ-irradiation process. The as-prepared RGO-Ni hybrid material shows greatly enhanced electromagnetic absorption ability than RGO at higher frequencies, due to the introduction of magnetic loss. A maximum RL value of -40 dB is found at 16.6 GHz for RGO-Ni, and all RL values are higher than -10 dB in the frequency range of 14.2-18 GHz. EM absorption of RGO-Ni originates from a synergetic consequence of dielectric loss, magnetic loss and improved impedance matching. We believe the as-described γ-irradiation induced reduction technique will be appealing for the fabrication of RGO-metal nanocomposites for various applications.

We acknowledge the financial supports from China Postdoctor Fund (2013M530149) and Heilongjiang Postdoctor Fund, Natural Science Foundation of China (No. 21203045, 21101041, 21003029, 21371039, 51377048), Fundamental Research Funds for the Central Universities (Grant No. HIT. NSRIF. 2010065 and 2011017, and HIT.BRETIII. 201223), and Scientific Research Foundation for Young Scientist of Harbin (2012RFQYG117, 2013RFQYG170).

Notes and references

[a]Fundamental Science on Nuclear Safety and Simulation Technology Laboratory, Harbin Engineering University, Harbin 150009, China.
[b]HIT-HAS Laboratory of High-Energy Chemistry and Interdisciplinary Science, Harbin Institute of Technology, Harbin 150001, China. Email: pxu@hit.edu.cn; zhaohongtao1976@163.com;lzg0015@163.com
[c]Institute of Technical Physics, Heilongjiang Academy of Sciences, Harbin 150009, China.

† Electronic Supplementary Information (ESI) available: Experimental details, Fig. S1-S4. See DOI: 10.1039/c000000x/

1. J. Guo, X. Wang, X. Liao, W. Zhanga and B. Shi, *The Journal of Physical Chemistry C*, 2012, **116**, 8188-8195.
2. G. Sun, B. Dong, M. Cao, B. Wei and C. Hu, *Chemistry of Materials*, 2011, **23**, 1587-1593.
3. H.-B. Zhang, Q. Yan, W.-G. Zheng, Z. He and Z.-Z. Yu, *ACS Applied Materials & Interfaces*, 2011, **3**, 918-924.
4. C.-L. Zhu, M.-L. Zhang, Y.-J. Qiao, G. Xiao, F. Zhang and Y.-J. Chen, *The Journal of Physical Chemistry C*, 2010, **114**, 16229-16235.
5. Z. W. Li, Z. H. Yang and L. B. Kong, *Journal of Applied Physics*, 2011, **110**, -.
6. F. Wang, J. Liu, J. Kong, Z. Zhang, X. Wang, M. Itohb and K.-i. Machida, *J Mater Chem*, 2011, **21**, 4314-4320.
7. C. Wang, X. J. Han, P. Xu, J. Y. Wang, Y. C. Du, X. H. Wang, W. Qin and T. Zhang, *J Phys Chem C*, 2010, **114**, 3196-3203.
8. R. Lv, F. Kang, J. Gu, X. Gui, J. Wei, K. Wang and D. Wu, *Appl. Phys. Lett.*, 2008, **93**, -.
9. V. Georgakilas, M. Otyepka, A. B. Bourlinos, V. Chandra, N. Kim, K. C. Kemp, P. Hobza, R. Zboril and K. S. Kim, *Chemical Reviews*, 2012, **112**, 6156-6214.
10. Y. Chen, Z. Lei, H. Wu, C. Zhu, P. Gao, Q. Ouyang, L.-H. Qi and W. Qin, *Materials Research Bulletin*, 2013, **48**, 3362-3366.
11. X. Li, H. Yi, J. Zhang, J. Feng, F. Li, D. Xue, H. Zhang, Y. Peng and N. Mellors, *J Nanopart Res*, 2013, **15**, 1-11.
12. C. Wang, X. J. Han, P. Xu, X. L. Zhang, Y. C. Du, S. R. Hu, J. Y. Wang and X. H. Wang, *Appl Phys Lett*, 2011, **98**, 072906.
13. C. Bao, L. Song, W. Xing, B. Yuan, C. A. Wilkie, J. Huang, Y. Guo and Y. Hu, *Journal of Materials Chemistry*, 2012, **22**, 6088-6096.
14. A. R. Anderson and E. J. Hart, *The Journal of Physical Chemistry*, 1962, **66**, 70-75.
15. J. L. Marignier, J. Belloni, M. O. Delcourt and J. P. Chevalier, *Nature*, 1985, **317**, 2.
16. G. E. Boris, *Russian Chemical Reviews*, 2004, **73**, 101.
17. E. D. Grayfer, A. S. Nazarov, V. G. Makotchenko, S.-J. Kim and V. E. Fedorov, *Journal of Materials Chemistry*, 2011, **21**, 3410-3414.
18. Z.-J. Fan, W. Kai, J. Yan, T. Wei, L.-J. Zhi, J. Feng, Y.-m. Ren, L.-P. Song and F. Wei, *ACS Nano*, 2010, **5**, 191-198.

19. X. H. Huang, Z. Y. Zhan, X. Wang, Z. Zhang, G. Z. Xing, D. L. Guo, D. P. Leusink, L. X. Zheng and T. Wu, *Appl Phys Lett*, 2010, **97**, 203112.
20. S. Stankovich, D. A. Dikin, R. D. Piner, K. A. Kohlhaas, A. Kleinhammes, Y. Jia, Y. Wu, S. T. Nguyen and R. S. Ruoff, *Carbon*, 2007, **45**, 1558-1565.
21. W. Y. Li, J. G. Liu and C. W. Yan, *Carbon*, 2013, **55**, 313-320.
22. Y. X. Xu, H. Bai, G. W. Lu, C. Li and G. Q. Shi, *J Am Chem Soc*, 2008, **130**, 5856-+.
23. Z. G. Wang, Y. Hu, W. L. Yang, M. J. Zhou and X. Hu, *Sensors-Basel*, 2012, **12**, 4860-4869.
24. X. Sun, J. He, G. Li, J. Tang, TaoWang, Y. Guo and H. Xue, *Journal of Materials Chemistry C*, 2013, **1**, 765-777.
25. P. Xu, X. J. Han, J. J. Jiang, X. H. Wang, X. D. Li and A. H. Wen, *J Phys Chem C*, 2007, **111**, 12603-12608.
26. M. Zong, Y. Huang, H. W. Wu, Y. Zhao, Q. F. Wang and X. Sun, *Mater Lett*, 2014, **114**, 52-55.
27. L. Wang, Y. Huang, X. Sun, H. J. Huang, P. B. Liu, M. Zong and Y. Wang, *Nanoscale*, 2014, **6**, 3157-3164.
28. R. C. Che, L.-M. Peng, X. F. Duan, Q. Chen and X. L. Liang, *Advanced Materials*, 2004, **16**, 401-405.

